Composites Part B, 42:41–50, 2011.

A Robust Three-node Shell Element for Laminated Composites with Matrix Damage

G. Sgambitterra[1]
Università della Calabria, Italy.
and
A. Adumitroaie[2] and E. J. Barbero[3]
Mechanical and Aerospace Engineering, West Virginia University,
Morgantown, WV 26506-6106, USA
and
A. Tessler[4]
NASA Langley Research Center, USA.

Abstract

A constitutive model for laminated composite shells with transverse matrix damage and its associated shell constitutive equations in three-dimensional space are developed. A single, physically relevant state variable is used in each lamina to track the state of transverse damage. The state variable also defines a physically relevant, solution dependent, characteristic length for the problem. Therefore, the constitutive model does not introduce constitutive mesh dependency on the solution. The model predicts crack initiation and evolution in good agreement with published experimental results for several materials and many different laminate stacking sequences. Input material parameters are limited to elastic properties and fracture toughness in mode I and II. Unlike continuum damage mechanics models, no adjustable parameters are needed to describe the initiation and evolution of damage. That is, the material parameters needed for the analysis are limited to invariant material properties that can be measured with standard test methods. The excellent predictive capabilities of the model and its versatility of application to a variety of materials and laminate configurations hinges upon computation of energy release rate for the entire laminate as a results of cracks propagating in any one lamina. Such computation requires knowledge about the state variables in all laminae when computing damage evolution in any one lamina, which in turn requires implementation of the constitutive equations directly into the element formulation. Therefore, the constitutive model is integrated into a shell element based on 1,2-order shell theory, and further implemented as a user element into commercial finite element analysis software.

[1]Postdoctoral research associate, Corresponding author. e-mail: gsgambitterra@libero.it. The final publication is available at http://dx.doi.org/10.1016/j.compositesb.2010.09.016
[2]Graduate Research Assistant
[3]Professor
[4]Senior Research Scientist

Keywords

B. Transverse cracking; C. Damage mechanics; C. Finite element analysis (FEA)

1 Introduction

Optimum utilization of composite materials is achieved when the geometry is designed so that the material resists the loads primarily through membrane stresses [1]. This leads naturally to curved shell geometries that also are more aesthetically pleasing than flat panel assemblies and to savings in part count by consolidating a number of parts and subassemblies into fewer curved shell structures. It is therefore necessary employ analysis tools capable of predicting the structural and material response up to failure for these situations.

Such design requires knowledge of at least two laminate response values, the first ply failure (FPF) strength and the last ply failure (LPF) strength [1]. FPF indicates the load at which the first ply in the laminated shell reaches a damage mode, usually matrix cracking. With proper laminate design, FPF does not precipitate laminate failure, but the presence of matrix cracks has several detrimental effects on the performance of the structure. Matrix cracks increase the permeability of the laminate, which can no longer prevent the ingress or egress of fluids and gases. Mass transport, either gas or fluid, may carry deleterious chemicals, including moisture, that may then attack the fibers, specially Glass fibers, thus reducing the life of the structure. Matrix cracks further reduce the fatigue life of the laminate, and may promote delaminations and fiber breaks in adjacent laminae. Finally, the stiffness reduction due to matrix cracks causes stress redistribution into adjacent laminae that then may precipitate fiber-dominated damage modes in those laminae and thus failure of the laminate.

Last Ply Failure (LPF) indicates a prediction of the ultimate load carrying capacity of the laminate. It is usually associated to fiber-dominated damage modes, although poorly designed laminates may reach LPF on matrix-dominated damage modes as well. Constitutive models exist for fiber-dominated damage modes [1, 2] that are able to predict accurately the strength of the unidirectional lamina along the fiber direction provided that a good estimate of the longitudinal stress (or strain) in the lamina is available. For this reason, it is critical to model accurately the stiffness reduction in cracking laminae so that stress redistribution onto the longitudinal direction of adjacent laminae is predicted accurately.

FPF is customarily predicted using stress (or strain) failure criteria [1]. The transverse strength F_{2t} and shear strength F_6 of the unidirectional lamina are measured with standard test methods. Then, the values are adjusted, ply by ply, to account for the constraining effect of adjacent laminae, yielding ply-thickness dependent values of in-situ strength $F^{(k)}_{2t-is}$, $F^{(k)}_{6-is}$, where k is the ply (lamina) number [3]. In this way, failure criteria such as maximum stress or interacting failure criteria [1] are able to predict the first matrix crack initiation in a ply. Due to the constraining effect of adjacent laminae, matrix crack initiation does not imply crack saturation, and thus stress redistribution to adjacent laminae is not properly accounted.

Once FPF has been predicted, ply discount methods are sometimes used to discount, or to degrade by an arbitrary factor d_f, the stiffness of affected ply. Stress redistribution is thus suddenly felt by adjacent laminae and another linear-elastic analysis is carried out to predict the next FPF. A sequence of such discounts eventually triggers a fiber-dominated damage mode prediction, which is then considered to correspond to the LPF of the laminate. Due in part to the arbitrariness of the value degradation factor used, the ply discount method has not gained acceptance in the design community.

Another approach is to use continuum damage mechanics (CDM) to represent stiffness degradation with representative damage variables and to fit the evolution of those damage variables with *postulated* evolution equations [2, Chapter 8]. The drawback of this method is the need to adjust the values of several new parameters with experimental data [4,5]. These parameters appear in the postulated evolution equations and the experimental data required to adjust them is seldom available. Therefore, there is strong motivation to develop predictive methods based on available material properties, perhaps supplemented by well defined material properties that can be determined by experimental methods that are either standardized or that are amenable to standardization [6, ASTM D 5528], [7,8].

Using finite fracture mechanics [9–11], several models have been developed that predict the stiffness reduction of a laminate as a function of a *given* crack density in one of its laminae. In [12,13] the laminate stacking sequence (LSS) is restricted to $[0/90_n]_S$ and in [14,15] to $[0_m/90_n]_S$. In [16] it is restricted to $[\pm\theta, 90_n]_S$, but only the 90° ply can experience damage. In [17] the LSS is restricted to $[\theta_n/\phi_m]_S$ with cracks on both directions. In [18] the LSS is restricted to $[0/45]_S$. In [19] a solution is presented for two sets of arbitrarily oriented cracking laminae with angles θ_1, θ_2 and crack densities λ_1, λ_2, embedded in a laminate with arbitrary LSS, by using oblique coordinates.

A finite-strip method is used in [20] to predict laminate stiffness reduction in a general unsymmetrical LSS due to a *given* crack density in a single ply. A model based on crack opening displacement (COD) [21] is able to predict laminate stiffness reduction due to *given* distribution of crack densities in all laminae of a laminate with general LSS. A damage activation function (growth criterion) for the same model is proposed in [22]. Symmetric laminates with in-plane loads are analyzed in [23, 24]. Damage evolution due to microcracking, after the first occurrence of failure, can be also modeled by means of a mesomechanical approach which takes into account the effect of microcracks in an average sense. For instance, the mechanical behavior of bimodular laminated composites damaged by an anisotropic distribution of cracks, has been studied determining the microstructure state of the material in terms of an opportune constitutive law taking into account for stiffness degradation in the context of the self-consistent micromechanical approach [25].

Although stress-based and strain-based failure criteria with ply values adjusted for in-situ effects [3] can predict damage (crack) initiation, they cannot predict damage evolution. Therefore, the crack density needed by the aforementioned models is not readily available as function of the applied strain (or stress). In order to overcome the aforementioned limitations of existing models, a solution for the general problem of curved, laminated shells, is presented herein. The proposed formulation has been developed by integrating the constitutive model into a shell element, as described next.

2 Element Formulation

A three-node flat shell element based on 1,2-order shell theory [26] is used herein. The formulation includes all six strain and stress components, including transverse shear and transverse normal deformations. The three-node element is based on quadratic anisoparametric displacements and linear bending rotation variables, giving rise to three displacements and three rotations at each vertex node. The element is readily portable to any general purpose finite element code and, in the present work, the element software is implemented as a user element into ANSYS [27]. The kinematic assumptions of 1,2-order shell theory can be expressed in terms of the Cartesian displacement components as

$$
\begin{aligned}
u_1(x_1, x_2, x_3) &= u + x_3\theta_2 \\
u_2(x_1, x_2, x_3) &= v + x_3\theta_1 \\
u_3(x_1, x_2, x_3) &= w + \xi w_1 + \left(\xi^2 - \tfrac{1}{5}\right) w_2
\end{aligned} \tag{1}
$$

where h denotes the shell thickness, $\xi = 2\,x_3/h \in [-1, 1]$ is a dimensionless thickness coordinate, with $\xi = 0$ identifying the midplane position; $u = u(x_1, x_2)$ and $v = v(x_1, x_2)$ are respectively the midplane displacements along the x_1 and x_2 axes; $\theta_1 = \theta_1(x_1, x_2)$ and $\theta_2 = \theta_2(x_1, x_2)$ are the rotations of the normal about the negative x and positive y directions, respectively; and $w = w(x_1, x_2)$, $w_1 = w_1(x_1, x_2)$, and $w_2 = w_2(x_1, x_2)$ are the three components of the transverse displacement, providing a parabolic distribution through the thickness.

Additional approximations involve parabolic transverse shear strains and cubic transverse normal stress, that are given as

$$
\begin{aligned}
\gamma_{13} &= \tfrac{5}{4}\left(1 - \xi^2\right)\,\gamma_{10} \\
\gamma_{23} &= \tfrac{5}{4}\left(1 - \xi^2\right)\,\gamma_{20} \\
\sigma_{33} &= \sigma_{30} + \left(\xi - \tfrac{1}{3}\xi^3\right)\,\sigma_{31}
\end{aligned} \tag{2}
$$

These quantities are average representations of the transverse shear strain and transverse normal stress; they satisfy traction equilibrium equations on the top and bottom shell surfaces, manifested by zero normal and shear tractions

$$
\begin{aligned}
\sigma_{33,3}\left(\pm\tfrac{h}{2}\right) &= 0 \\
\tau_{13}\left(\pm\tfrac{h}{2}\right) = \tau_{23}\left(\pm\tfrac{h}{2}\right) &= 0
\end{aligned} \tag{3}
$$

By enforcing the strain-displacement relations

$$
\begin{aligned}
\gamma_{13} &= u_{1,3} + u_{3,1} \\
\gamma_{23} &= u_{2,3} + u_{3,2} \\
\varepsilon_{33} &= u_{3,3}
\end{aligned} \tag{4}
$$

to be least-squares compatible through the shell thickness with the corresponding strains resulting from (2), the pair $[\gamma_{10}\,, \gamma_{20}] = [w_{,1} + \theta_2\,, w_{,2} + \theta_1]$ define the transverse shear strain measures, whereas σ_{30} and σ_{31} become functions of the inplane strains $[u_{,1}\,, v_{,2}\,, u_{,2} + v_{,1}]$ and curvatures $[\theta_{2,1}\,, \theta_{1,2}\,, \theta_{1,1} + \theta_{2,2}]$.

As a result of these approximations, the two-dimensional virtual work statement does not include the higher-order transverse displacement variables (w_1, w_2); these variables are condensed out analytically from the pertinent shell-equilibrium equations [26, 28]. The remaining five kinematic variables are the same as those of first-order shear deformation theory, only needing edge continuity for their approximation within the finite element framework.

In the finite element formulation, the three displacement variables (u, v, w) are initially interpolated with quadratic, six-node polynomials, whereas the two bending rotations are interpolated with linear, three-node shape functions. In addition to achieving improved membrane response (i.e., linear inplane strain), using the same degree polynomial interpolations for the three displacement

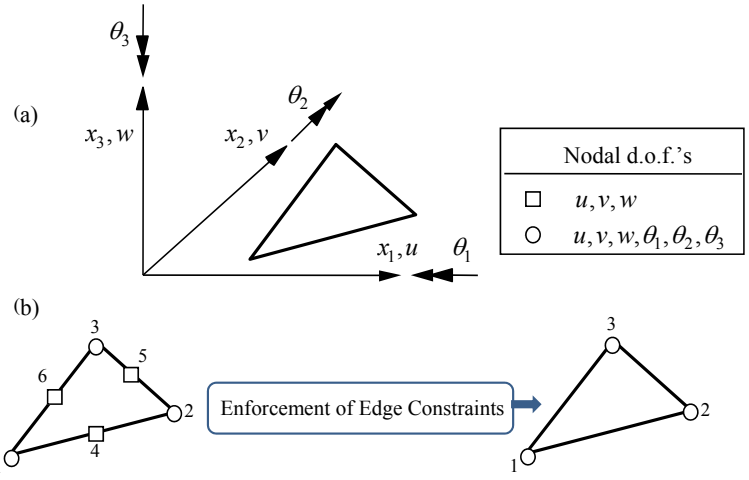

Figure 1: Notation for HOT3D shell element: (a) kinematics; (b) nodal d.o.f's reduction.

variables ensures displacement compatibility along the element interfaces. The mid-side displacement degrees-of-freedom (d.o.f.'s) are then condensed out by enforcing a set of first-order Kirchhoff constraints along the three element edges via beam-frame one-dimensional constraint conditions, thus reducing the number of nodes to three (refer to Fig. 1).

The edge-constraint procedure gives rise to a new set of interpolations, where the inplane displacements (u, v) contain both the inplane and normal rotation (drilling) d.o.f.'s, and the deflection w contains both the deflection and bending rotation d.o.f.'s. The resulting kinematic field involves a compatible set of shape functions with three translations and three rotation d.o.f.'s at each vertex node. The element is thus labeled HOT3D (Higher-Order Theory, 3 nodes, Drilling d.o.f.'s) [29].

The parabolic transverse displacement and the linear bending rotations ensure a consistent set of interpolations for the bending behavior, providing adequate element performance without shear-locking stiffening in thin shells. Further improvements in the thin-shell modeling are due to the use of strain-energy derived relaxation parameters that appear as the scaling factors of the transverse-shear strain measures. This methodology guarantees a well-conditioned element stiffness matrix over the entire range of thickness-to-span ratios [29]. Finally, the element matrices are integrated exactly using appropriate quadrature formulas for triangular elements in order to maintain variational consistency and a correct rank of the element stiffness matrix. The formulation is well suited for the computation of both in-plane and out-of-plane shear and normal stress-strain components, making in this way possible the utilization of three dimensional failure criteria, in order to predict multiple modes of failure, as matrix cracking (intralaminar failure) or delamination (interlaminar failure). However, the present model is dedicated to matrix cracking (intralaminar) failure mode. Furthermore, only modes I (the opening mode) and II (the in-plane shearing mode) of matrix cracking are considered in here, as the ones that are more probable to take place in structural elements based on shell laminated composites, which are not primarily designed to stand high transverse shear loads that would produce mode III matrix cracking. These are the reasons why the interlaminar shear and normal stress components are not used in the failure criterion implemented in the present model, which is introduced in Section 4.

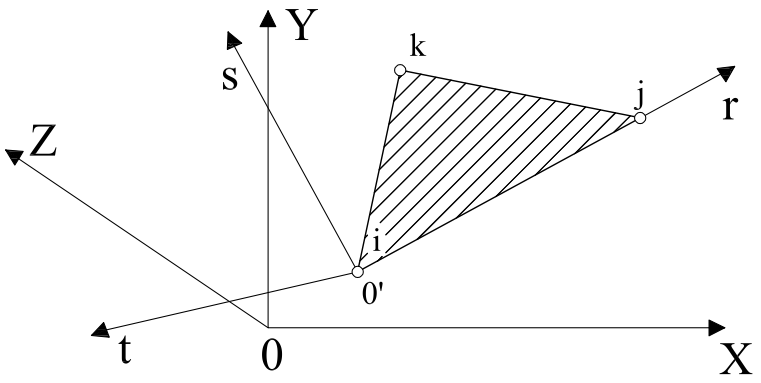

Figure 2: Global coordinate system (X,Y,Z) and local coordinate system (r,s,t).

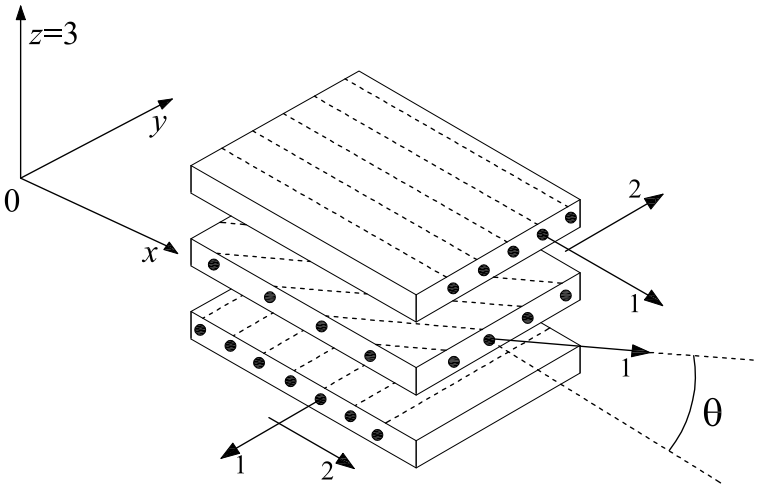

Figure 3: Material (1-2-3) and laminate *(x,y,z)* coordinate system.

3 Laminated-Shell Constitutive Model

In a finite element code for isotropic materials, only two coordinate systems are needed: the *global* coordinate system (X,Y,Z) and the *element* coordinate system (r,s,t) shown in Figure 2. In a shell element for *laminated composites*, two additional coordinate systems are needed: the *material* coordinate system (1,2,3) for each lamina and the *laminate* coordinate system *(x,y,z)* (Figure 3). The laminate stacking sequence (LSS) includes the thickness and orientation $\theta^{(k)}$ of each lamina k with respect the laminate coordinate system, as shown in Figure 3.

Transformation from the global (X,Y,Z) to the laminate *(x,y,z)* coordinate system requires specification of the orientation of the laminate coordinate system for each element. In this work, this is accomplished by specifying three Euler angles per element. Although these three angles can be defined in a number of ways, herein they are defined consistently with the angles used in ANSYS$^{\text{TM}}$ for the specification of `LOCAL` coordinate systems [27]. Note that in this work, the *element* coordinate system refers to the coordinate system utilized for element formulation, whereas the *laminate* coordinate system (commonly referred to as *local*) refers to the reference system used to specify the angles in the laminate stacking sequence. For the triangular element used, the *element* system is defined by the orientation of the first two nodes in the element connectivity, labeled *i,j,* in Figure 2. Since the mesh generation is customarily done by automated means, the *element* system

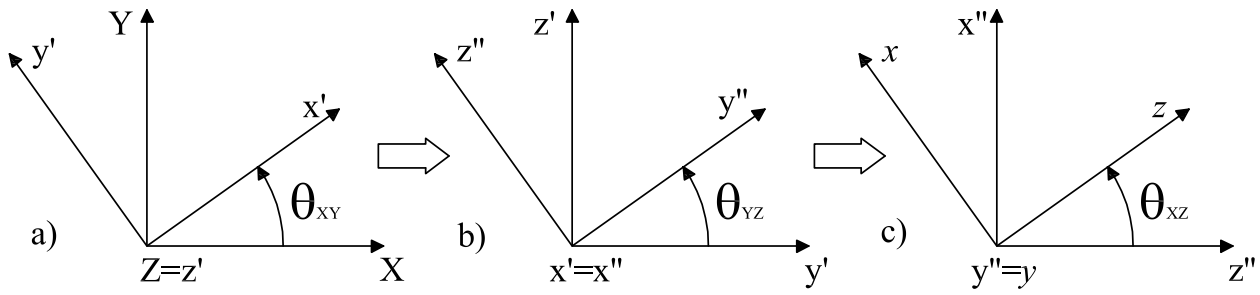

Figure 4: Rotation around the axes z', x', and y" to transform from the global coordinate system (X,Y,Z) to the laminate coordinate system *(x,y,z)*.

is not a convenient choice for specifying the material orientation. Thus, a separate *laminate* system is defined. The three rotations, denoted by $\theta_{xy}, \theta_{yz}, \theta_{xz}$, are performed in sequence around the rotated axes z′, x′, and y″ as shown in Figure 4 to arrive at the laminate coordinate system x, y, z. This transformation is used to transform strains, stress, and the material compliance and stiffness matrices from the global coordinate system to the laminate coordinate system, or vice versa. The transformation matrices are shown in the Appendix.

The element and associated constitutive model are implemented as a user element in ANSYS. The main program interacts with the user element one element at a time. It provides the nodal coordinates and current nodal displacements, both expressed in the global coordinate system. It requires the user element to compute the current stress, the element stiffness and the force vector. Since the constitutive equation is non-linear, and the nonlinearity is formulated in terms of state variables, the main program stores the state variables and provides them to the user element. All computations related to material behavior and coordinate transformations needed to properly take into account the orientation of both, element and material, in three-dimensional space, are performed inside the user element.

Given a set of element nodal displacements $\{X^G\}$ in the *global* coordinate system, these are first transformed to the *element* coordinate system $\{x^E\}$. The required transformation matrix $[a^E]$ from the *global* (G) coordinate system to the *element* element (E) coordinate system contains the direction cosines of the element (local) coordinate system (r,s,t,) w.r.t the global system (X,Y,Z.) Then, the local displacements are used to compute the strains $\{\epsilon^E\}$ at each Gauss integration point, also in the element coordinate system, as $\{\epsilon^E\} = [B]^T\{x^E\}$, where $[B]$ is the strain displacement matrix [30]. Since the constitutive model is cast in terms of the strain $\{\epsilon^L\}$ in the laminate coordinate system, the strain is transformed as follows

$$\{\varepsilon^L\} = [T^{eL}]\ [T^{sE}]^T\ \{\varepsilon^E\} \tag{5}$$

where $[T^{eL}]$ is given by (34), formulated in terms of the Euler angles used to specify the *laminate* coordinate system, and $[T^{sE}]$ is obtained by substituting $[a^E]$ for $[a]$ in (33), formulated in terms of the element nodal coordinates.

Given a state of strain, the constitutive model updates the state variables (crack densities $\lambda^{(i)}$ for the n laminae, with $i = 1...n$), the state of stress $\sigma^{(i)}$ and the reduced moduli in the laminae $E^{(i)}(\lambda^i)$. Since the element is able to compute all the strain components, including the through-the-thickness strain ϵ_3, the full compliance matrix $[S^M]$ and stiffness $[C^M]$ are assembled for each lamina k, in the material (M) coordinate system of the lamina [2, (1.54)]

$$[C^M] = [S^M]^{-1} = \begin{bmatrix} 1/E_1 & -\nu_{21}/E_2 & -\nu_{31}/E_3 & 0 & 0 & 0 \\ & 1/E_2 & -\nu_{32}/E_3 & 0 & 0 & 0 \\ & & 1/E_3 & 0 & 0 & 0 \\ & & & 1/G_{23} & 0 & 0 \\ & & & & 1/G_{13} & 0 \\ symm & & & & & 1/G_{12} \end{bmatrix}^{-1} \tag{6}$$

This is then transformed to the laminate coordinate system using a rotation $-\theta^{(k)}$ around the 3-axis of the laminate coordinate system, i.e, substituting $\theta^{(k)}$ for θ_{xy} and $\theta_{yz} = \theta_{xz} = 0$ in (28–30), yielding the lamina stiffness matrix in laminate coordinates $[C^L]$ as [2, (1.49)]

$$[C^L] = [T(\theta)]^T \; [C^M] \; [T(\theta)] \tag{7}$$

The element formulation needs the laminate stiffness matrix $[D^E]$, defined in (9) below, to be expressed in the element coordinate system in order to formulate the element stiffness matrix as the integral of terms $[B]^T[D^E][B]$, where $[B]$ is the strain-displacement matrix [30]. Therefore, the stiffness matrix $[C^L]$ from (7) is transformed to element coordinates as follows

$$[C^E] = [T^{sE}] \; [T^{eL}]^T \; [C^L] \; [T^{eL}] \; [T^{sE}]^T \tag{8}$$

Then, the laminate stiffness matrix $[D^E]$ is built in the element coordinate system by performing an analytical integration through-the-thickness x_3 of the laminate, that yields

$$\{\mathrm{N}\} = \left[D^E\right] \{\varepsilon\}$$

$$\begin{Bmatrix} N_r \\ N_s \\ N_{rs} \\ M_r \\ M_s \\ M_{rs} \\ V_{st} \\ V_{rt} \end{Bmatrix} = \begin{bmatrix} A_{11} & A_{12} & A_{16} & B_{16} & B_{12} & B_{16} & 0 & 0 \\ A_{12} & A_{22} & A_{26} & B_{12} & B_{22} & B_{26} & 0 & 0 \\ A_{16} & A_{26} & A_{66} & B_{16} & B_{26} & B_{66} & 0 & 0 \\ B_{11} & B_{12} & B_{16} & D_{11} & D_{12} & D_{16} & 0 & 0 \\ B_{12} & B_{22} & B_{26} & D_{12} & D_{22} & D_{26} & 0 & 0 \\ B_{16} & B_{26} & B_{66} & D_{16} & D_{26} & D_{66} & 0 & 0 \\ 0 & 0 & 0 & 0 & 0 & 0 & H_{44} & H_{45} \\ 0 & 0 & 0 & 0 & 0 & 0 & H_{45} & H_{55} \end{bmatrix} \begin{Bmatrix} \varepsilon_r^0 \\ \varepsilon_s^0 \\ \gamma_{rs}^0 \\ k_r \\ k_s \\ k_{rs} \\ \gamma_{st} \\ \gamma_{rt} \end{Bmatrix} \tag{9}$$

where explicit expressions for the $A_{ij}-, B_{ij}-, D_{ij}-, H_{ij}-$terms are given in [29, Appendix B].

4 Damage Constitutive Model

As stated in the previous section, given a state of strain, the constitutive model's purpose is to update the state variables (crack densities), then update the stress and the reduced moduli in each lamina. A constitutive model for a continuum (not discretized) solution at a single material point of a plane stress problem with uniform uni-axial loading was presented in [31], where the crack density as a function of strain (stress) is predicted. A finite element implementation for a plane-stress element is presented in [32]. However, a plane stress implementation cannot be used with shell elements in commercial finite element analysis (FEA) codes via the user material option, as explained next.

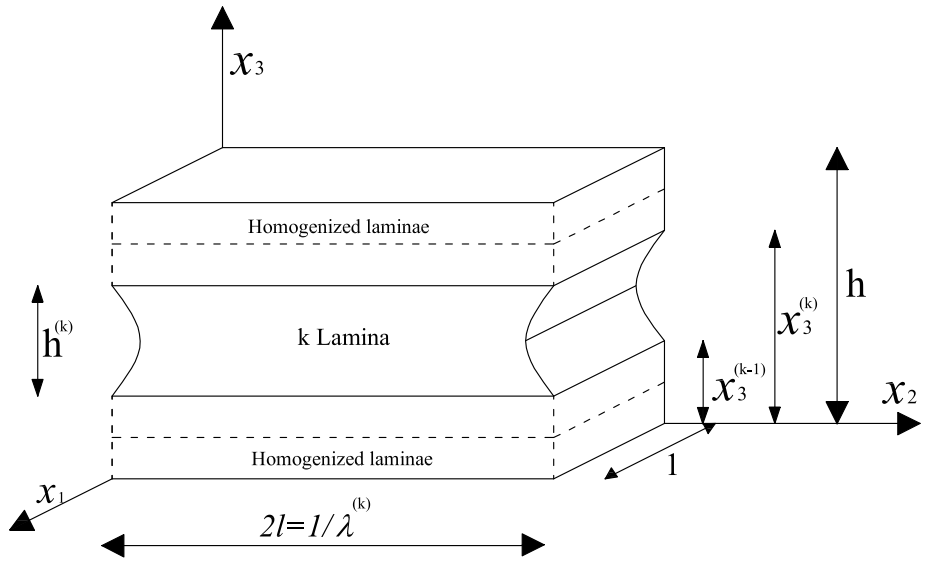

Figure 5: Representative volume element (RVE) in the coordinate system x_1, x_2, x_3, of lamina k.

Commercial codes perform numerical integration through the thickness of the shell to calculate the laminate constitutive matrix. For each lamina, they call a plane-stress constitutive model; however they do not provide, to the user material routine, the state variables for the remaining laminae in the laminate. In other words, the plane-stress constitutive model used in commercial codes is local to the lamina. Such approach is well suited for failure criteria that are local to the lamina, because their coupling to the rest of the laminae is provided by the stress-strain field only. By contrast, the constitutive model presented in this section requires access to the state variables for all laminae in order to compute accurately the *energy release rate* (ERR) from strain energy released throughout the laminate. Therefore, analytical integration through-the-thickness is used in this work to arrive at a constitutive model for the laminate that can be used in the user-implemented shell finite element described herein. Furthermore, coordinate transformations are developed to cast the constitutive model for the orthotropic laminate in the correct orientation when the shell elements are oriented arbitrarily in three-dimensional space.

The proposed constitutive model is based on a shear lag solution in a representative volume element (RVE) and a homogenization scheme used to analyze arbitrary laminate stacking sequences (LSS). The model takes into account thermal expansion and associated residual stresses but only the mechanical terms are included in the presentation that follows in order to keep the manuscript to a reasonable length; nevertheless, the thermal expansion terms can be derived in an analogous

way [2].

Shear lag solutions, applied to less general problems, are available in the literature [12, 13, 17, 19, 31, 33, 34]. One advantage of constitutive models based on RVE is that the state variable (crack density) uniquely defines the characteristic length of the finite fracture mechanics problem. For the present constitutive model, the size of the RVE (Figure 5) is the inverse of the crack density. Unlike continuum (smeared) fracture models, there is no need in the present model to introduce an artificial characteristic length to avoid constitutive mesh dependency. The RVE-based constitutive model developed herein is mesh independent. Only the the mesh dependency introduced by the discretization has an effect on the quality of the stress and strain gradients and thus on the solution. This advantage is not significant in simple implementations of the constitutive models, for a single material point, such as in [31]; but is only noticed in finite element implementations such as in this work. Therefore, numerical results are presented in this manuscript to illustrate this feature.

For a single cracking lamina k, the shear lag method [31] provides an analytical solution for the displacement field in the RVE

$$\begin{Bmatrix} \hat{u}^{(1)} \\ \hat{u}^{(2)} \\ \vdots \\ \hat{u}^{(n)} \\ \hat{v}^{(1)} \\ \hat{v}^{(2)} \\ \vdots \\ \hat{v}^{(n)} \end{Bmatrix} = \sum_{j=1}^{2n} A_j \begin{bmatrix} a_1 \\ a_2 \\ \vdots \\ a_n \\ a_{n+1} \\ a_{n+2} \\ \vdots \\ a_{2n} \end{bmatrix}_j \sinh(\zeta_j x_2) + \begin{bmatrix} 1/2\gamma_{12}^c \\ 1/2\gamma_{12}^c \\ \vdots \\ 1/2\gamma_{12}^c \\ \varepsilon_2^c \\ \varepsilon_2^c \\ \vdots \\ \varepsilon_2^c \end{bmatrix} x_2 + \begin{bmatrix} \varepsilon_1^c \\ \varepsilon_1^c \\ \vdots \\ \varepsilon_1^c \\ 1/2\gamma_{12}^c \\ 1/2\gamma_{12}^c \\ \vdots \\ 1/2\gamma_{12}^c \end{bmatrix} x_1 \tag{10}$$

where $\hat{u}^{(k)}, \hat{v}^{(k)}$ are the average displacements in each lamina, in the coordinate system of the cracking lamina x_1, x_2, x_3, (Figure 5), with the averaging defined in lamina k by

$$\hat{\phi} = \frac{1}{h^{(k)}} \int_{x_3^{(k-1)}}^{x_3^{(k)}} \phi dx_3 \tag{11}$$

and x_1, x_2 are coordinates aligned with the material coordinate system of lamina k; ζ_j and $[a]_j$ $(j = 1 \cdots 2n)$ are the eigenvalues and the eigenvectors of the system, and $A_j, \varepsilon_1^c, \varepsilon_2^c, \gamma_{12}^c$, are unknown constants.

The laminate thickness is calculated as

$$h = \sum_{i=1}^{n} h^{(i)} \tag{12}$$

where n is the number of laminae.

Stress, displacement, and force equilibrium boundary conditions on the boundary of the RVE are used to calculate these constants. First, stress-free conditions at the surfaces of the cracks, in the cracking lamina k, yield

$$\begin{array}{ll} \frac{1}{2l} \int_{-1/2}^{1/2} \hat{\sigma}_2^{(k)} dx_1 = 0, & \text{at } x_2 = \pm l \\ \frac{1}{2l} \int_{-1/2}^{1/2} \hat{\tau}_{12}^{(k)} dx_1 = 0, & \text{at } x_2 = \pm l \end{array} \tag{13}$$

Second, for a symmetric laminate under membrane strain, force equilibrium between the internal stress in the un-cracked laminae and the applied in-plane stress resultant yield

$$\begin{array}{ll} \sum_{m=1}^{n}(1-\delta_{mk})h^{(m)}\int_{-1/2}^{1/2}\hat{\sigma}_2^{(m)}dx_1 = N_2, & \text{at } x_2=\pm l \\ \sum_{m=1}^{n}(1-\delta_{mk})h^{(m)}\int_{-1/2}^{1/2}\hat{\tau}_{12}^{(m)}dx_1 = N_{12}, & \text{at } x_2=\pm l \\ \sum_{i=1}^{n}\frac{h^{(i)}}{2l}\int_{-l}^{l}\hat{\sigma}_1^{(i)}dx_2 = N_1, & \text{at } x_1=\pm 1/2 \end{array} \tag{14}$$

Third, the kinematics of first order shear deformation theory (FSDT) dictates that, for a membrane state of deformation, the displacements in the x_2 direction be the same for all un-cracked laminae $m \neq k$

$$\begin{array}{llll} \int_{-1/2}^{1/2}\hat{u}^{(m)} = \int_{-1/2}^{1/2}\hat{u}^{(r)}, & \text{at } x_2=\pm l & \forall\ m,\ r\neq k \\ \int_{-1/2}^{1/2}\hat{v}^{(m)} = \int_{-1/2}^{1/2}\hat{v}^{(r)}, & \text{at } x_2=\pm l & \forall\ m,\ r\neq k \end{array} \tag{15}$$

where r is one reference lamina among the un-cracked m laminae.

Once the constants $\zeta_j, A_j, \varepsilon_1^c, \varepsilon_2^c, \gamma_{12}^c$, are found, the ply-average strains can be calculated by differentiation of (10), and the overall strains of the laminate can be calculated by selecting a reference un-cracked ply $r \neq k$ and considering the isostrain condition between the ply r and the whole laminate, as

$$\begin{array}{l} \bar{\varepsilon}_1 = \varepsilon_1^c \\ \bar{\varepsilon}_2 = \frac{1}{2l}\int_{-l}^{l}\hat{v}_{,2}^{(r)}\,dx_2 \\ \bar{\gamma}_{12} = \frac{1}{2l}\int_{-l}^{l}\left(\hat{u}_{,2}^{(r)} + \hat{v}_{,1}^{(r)}\right)dx_2 \end{array} \tag{16}$$

The laminate compliance matrix $[S]$ in the coordinate system of the cracking lamina k is obtained, one column at a time, by calculating the strains (16) corresponding to the three unit loads $N^{(a)} = \{N_1, 0, 0\}^T, N^{(b)} = \{0, N_2, 0\}^T, N^{(c)} = \{0, 0, N_{12}\}^T$, which yield

$$Q^{-1}(\lambda^{(k)}) = S(\lambda^{(k)}) = \left[\left\{ \begin{array}{c} \bar{\varepsilon}_1 \\ \bar{\varepsilon}_2 \\ \bar{\gamma}_{12} \end{array} \right\}^{(a)} \left\{ \begin{array}{c} \bar{\varepsilon}_1 \\ \bar{\varepsilon}_2 \\ \bar{\gamma}_{12} \end{array} \right\}^{(b)} \left\{ \begin{array}{c} \bar{\varepsilon}_1 \\ \bar{\varepsilon}_2 \\ \bar{\gamma}_{12} \end{array} \right\}^{(c)} \right] \tag{17}$$

Since the laminate stiffness $Q(\lambda)$ in the LHS of (17) may be written as the sum of the contributions of the cracking lamina k plus that of all the (for the moment) un-cracking laminae $m \neq k$, one can find the damaged stiffness of the cracking lamina k as

$$Q^{(k)}(\lambda^{(k)}) = \left[Q(\lambda^{(k)}) - \sum_{m}^{n-1} Q^{(m)}\frac{h^{(m)}}{h} \right] \frac{h}{h^{(k)}} \tag{18}$$

where h is the laminate thickness and n is the number of laminae.

Up to this point, finite fracture mechanics has been used to calculate the reduced properties of a laminate (17) and a *single* cracking lamina (18), for a given crack density $\lambda^{(k)}$.

Once $Q^{(k)}(\lambda^{(k)})$ is known, the discrete crack pattern characterized by crack density $\lambda^{(k)}$ can be homogenized, using concepts of continuum damage mechanics (CDM) [35–37], so that

$$Q^{(k)}(\lambda^{(k)}) = \begin{bmatrix} \overline{Q}_{11}^{(k)} & (1-D_{12}^{(k)})\overline{Q}_{12}^{(k)} & 0 \\ (1-D_{12}^{(k)})\overline{Q}_{12}^{(k)} & (1-D_{22}^{(k)})\overline{Q}_{22}^{(k)} & 0 \\ 0 & 0 & (1-D_{66}^{(k)})\overline{Q}_{66}^{(k)} \end{bmatrix} \tag{19}$$

where the damage parameters for lamina k are computed in terms of the analytic solution (17) and the undamaged (virgin) values $\overline{Q}_{ij}^{(k)}$ as follows,

$$D_{ij}^{(k)}(\lambda^{(k)}) = 1 - Q_{ij}^{(k)}/\overline{Q}_{ij}^{(k)} \tag{20}$$

with $i, j = 1, 2, 6$.

The homogenization process enabled by (20) permits the use of the shear lag solution (17) one lamina at a time, with previously cracked laminae simply converted to homogenized laminae with reduced properties. In this way, any LSS can be analyzed with any number of damaging laminae as required.

There still remains to find the crack density $\lambda^{(k)}$ as a function of applied strain $\bar{\varepsilon}$. To accomplish this, it is necessary to postulate a damage activation criterion [38], such as [39]

$$g(\lambda, \bar{\varepsilon}) = (1-r)\sqrt{\frac{G_I(\lambda,\bar{\varepsilon})}{G_{IC}}} + r\frac{G_I(\lambda,\bar{\varepsilon})}{G_{IC}} + \frac{G_{II}(\lambda,\bar{\varepsilon})}{G_{IIC}} - 1 \leq 0 \tag{21}$$

in terms of intralaminar fracture toughness G_{Ic}, G_{IIc} and ERR G_I, G_{II} in mode I and II.

The strain energy is separated naturally into mode I and II while working in the material coordinate system of the cracking lamina, as follows

$$U_I = \frac{V}{2}\left(\bar{\sigma}_1\bar{\varepsilon}_1 + \bar{\sigma}_2\bar{\varepsilon}_2\right) = \frac{V}{2}[\bar{\varepsilon}_1\left(Q_{11}\bar{\varepsilon}_1 + Q_{12}\bar{\varepsilon}_2 + Q_{16}\bar{\gamma}_{12}\right) + \bar{\varepsilon}_2\left(Q_{21}\bar{\varepsilon}_1 + Q_{22}\bar{\varepsilon}_2 + Q_{26}\bar{\gamma}_{12}\right)] \tag{22}$$

$$U_{II} = \frac{V}{2}\left(\bar{\tau}_{12}\bar{\gamma}_{12}\right) = \frac{V}{2}\bar{\gamma}_{12}\left(Q_{61}\bar{\varepsilon}_1 + Q_{62}\bar{\varepsilon}_2 + Q_{66}\bar{\gamma}_{12}\right) \tag{23}$$

where V is the volume of the RVE.

For most composites with brittle matrix, including most toughened epoxy matrices, cracks develop suddenly over a finite length [10, 11]. Even for laminates where cracks do not grow to span the width of the specimen, cracks still grow suddenly at first and occupying large areas of the specimen and the concept of crack density, as used in this manuscript, can still be applied [22]. Therefore, Griffith's energy principle is applied on its discrete (finite) form, in order to describe the discrete (finite) behavior of crack propagation observed experimentally, i.e.,

$$G_I = -\frac{\Delta U_I}{\Delta A} \tag{24}$$

$$G_{II} = -\frac{\Delta U_{II}}{\Delta A} \tag{25}$$

where $\Delta U_I, \Delta U_{II}$ is the change in laminate strain energy during mode I and II finite crack growth, and ΔA is the finite change of crack area.

The value of crack density $\lambda^{(k)}$ for which $g = 0$ in (21) is found with a return mapping algorithm that calculates the change in $\lambda^{(k)}$ as

$$\Delta\lambda^{(k)} = -g^{(k)} / \frac{\partial g^{(k)}}{\partial \lambda^{(k)}} \tag{26}$$

The damage activation function (21) is a monotonically decreasing function of $\lambda^{(k)}$ as a natural consequence of the decreasing moduli brought about by an increase in crack density. As soon as the crack density $\lambda^{(k)}$ increases, g decreases. The only way to reach $g = 0$ again is to increase the applied strain $\bar{\varepsilon}$. Thus, the damage activation function g calculated by the proposed model displays hardening without the need to postulate any hardening law. This has the clear advantage of obviating the need for additional experimentation that would otherwise be required to adjust hardening parameters that are necessarily associated with hardening laws.

Once the crack density and reduced moduli are found for all laminae, the computations are completed for a given strain $\bar{\varepsilon}$ and the algorithm returns to the element formulation described in the previous section.

	HyE 9082Af	Ref.	Fibredus 913G-E	Ref.	Hercules 3501-6/AS4	Ref.
E_1 (GPa)	44.7	[40]	46	[22]	130	[14]
E_2 (GPa)	12.7	[40]	18	[22]	9.7	[14]
ν_{12}	0.297	[40]	0.29	[22]	0.3	[14]
G_{12} (GPa)	5.8	[40]	7.9	[22]	5	[14]
G_{23} (GPa)	4.5	*	6.4	*	3.2	[14]
Ply thick (mm)	0.144	[40]	0.125	[22]	0.125	*
G_{Ic} (kJ/m^2)	0.36		0.40		0.05	
G_{IIc} (kJ/m^2)	1.50		1.50		1.50	
α_1 $(10^{-6}/°C)$	8.420	[1]	6.72	[22]	-0.09	[14]
α_2 $(10^{-6}/°C)$	0.184	[1]	0.293	[22]	0.288	[14]
ΔT $(°C)$	99	[1]	104	[22]	104	[14]

* Assumed value

Table 1: Material properties.

5 Numerical Results

In the first part of this section, predictions obtained with the proposed finite element formulation are presented and compared with experimental data from the literature for several laminate stacking sequences and three types of composites [14, 22, 40]. The material properties are summarized in Table 1. Interlaminar fracture toughness can be measured as in [6, ASTM D 5528] and [7, 8]. Since intralaminar fracture toughness is usually larger, E-glass–Epoxy values are assumed to be twice as large as known interlaminar values. Lacking experimental values of intralaminar fracture toughness for Carbon–Epoxy, the interlaminar fracture toughness (required by the model) was adjusted so that the model results provide the best fit possible to one LSS of experimental crack density vs. stress.

The first test case for a glass-epoxy material [40, Fiberite/HyE 9082Af], cross-ply laminate $[0/90_8/0_{1/2}]_S$, where cracks open in pure mode I. The experimental data was obtained at room

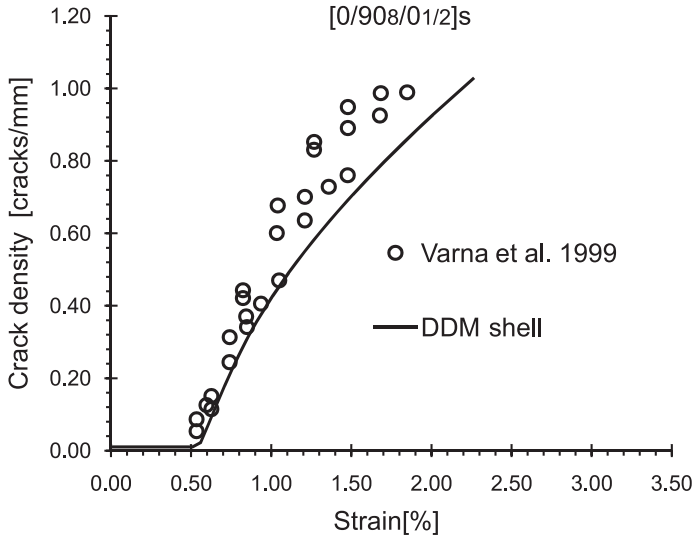

Figure 6: Crack density vs. strain for a $[0/90_8/0_{1/2}]_S$ laminate, $\Delta T = -99^oC$.

temperature and does not elucidate the effect of residual thermal stress; however the proposed formulation has the capability to predict the effect of residual thermal stresses. The strain required for crack initiation and evolution is shown in Figure 6. It is evident that the present predictions compare very well with the experimental data.

Using the same material, the cracks in a $[0/55_4/-55_4/0_{1/2}]_S$ laminate are subjected to both fracture modes I and II. Also, the analysis is carried out with and without the effect of residual thermal stress. The strain required for crack initiation and evolution is shown in Figure 7. The prediction is excellent when compared with the two sets of experimental data.

The next test case is for an E-glass/epoxy [22, Fibredux 913G-E], quasi-isotropic laminate $[0_n/90_n/+45_n/-45_n]_S$ with $n = 1, 2$. The prediction of the Young's Modulus versus the crack density in the 90° layer is excellent for $n = 2$ shown in Figure 8, but not as good for $n = 1$ in Figure 9. The reason for this is that additional damage in the form of delaminations is present for $n = 1$ [22], which the present formulation does not take into account. For $n = 2$, the laminae are thicker, delamination is less prominent, and the present predictions compare very well the experimental data.

The next test case is a graphite-epoxy [14, Hercules AS4/3501-6], cross-ply laminate. Crack density as a function of applied stress is compared in Figure 10, showing that the model predicts very well the stress required for crack initiation in the 90° layer.

To demonstrate the versatility of the proposed shell formulation, damage initiation and evolution is investigated on a complex shell structure. The case of an spherical shell with an 18° hole cutout at the top, subjected to internal pressure, is studied. In this example, the state of membrane deformation is predominant compared to bending. Due to symmetry, only one-eight of the shell is discretized (Figure 11). The laminate stacking sequence is $[0/90_8/0_{1/2}]_S$, and the material is a glass-epoxy [40, HyE 9082Af, Fiberite], which is the same laminate used to construct Figure 6. Euler angles were specified for each element via the ANSYS APDL `LOCAL` command to align the laminate x-axis along the meridians of the sphere. In this way, the 0° laminae are oriented along the meridian and the 90° lamina along the parallel. Symmetric boundary condition are applied along the sides and on the bottom of the model.

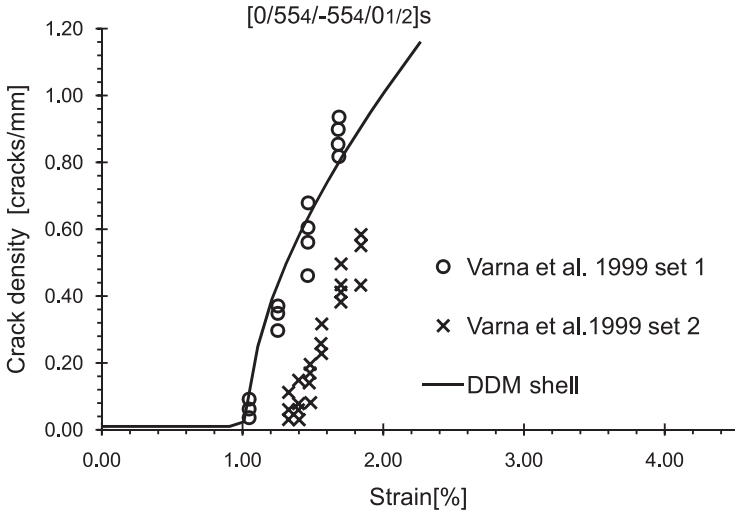

Figure 7: Crack density vs. strain for a $[0/55_4/-55_4/0_{1/2}]_S$ laminate, $\Delta T = -99^oC$.

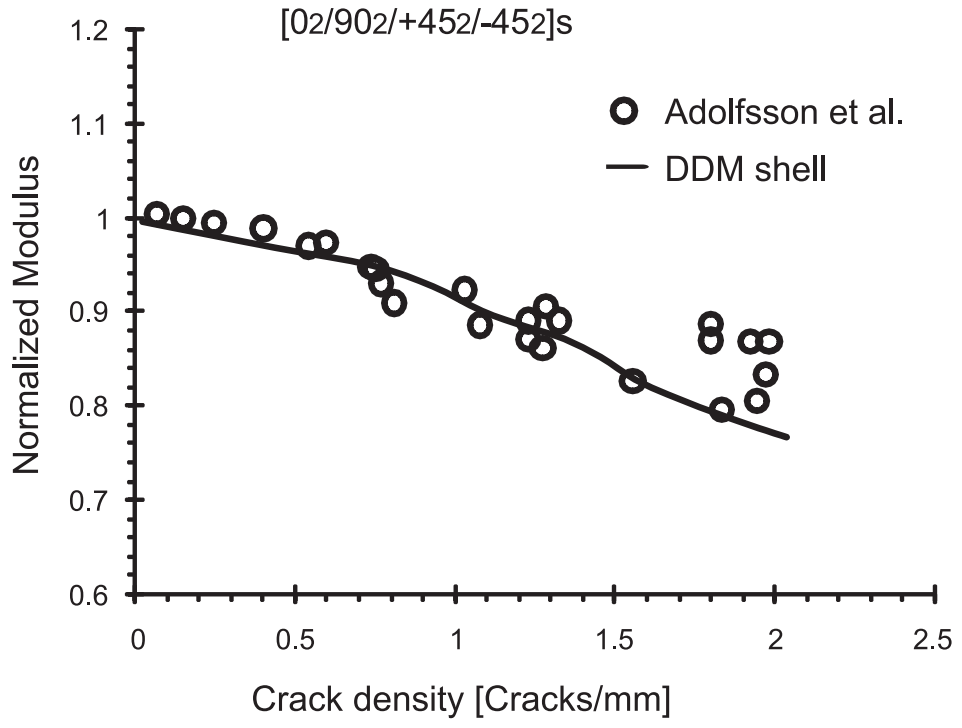

Figure 8: Normalized modulus $E_x/\bar{E}_x$ vs. crack density for a $[0_n/90_n/45_n/-45_n]_S$ laminate with $n = 2$.

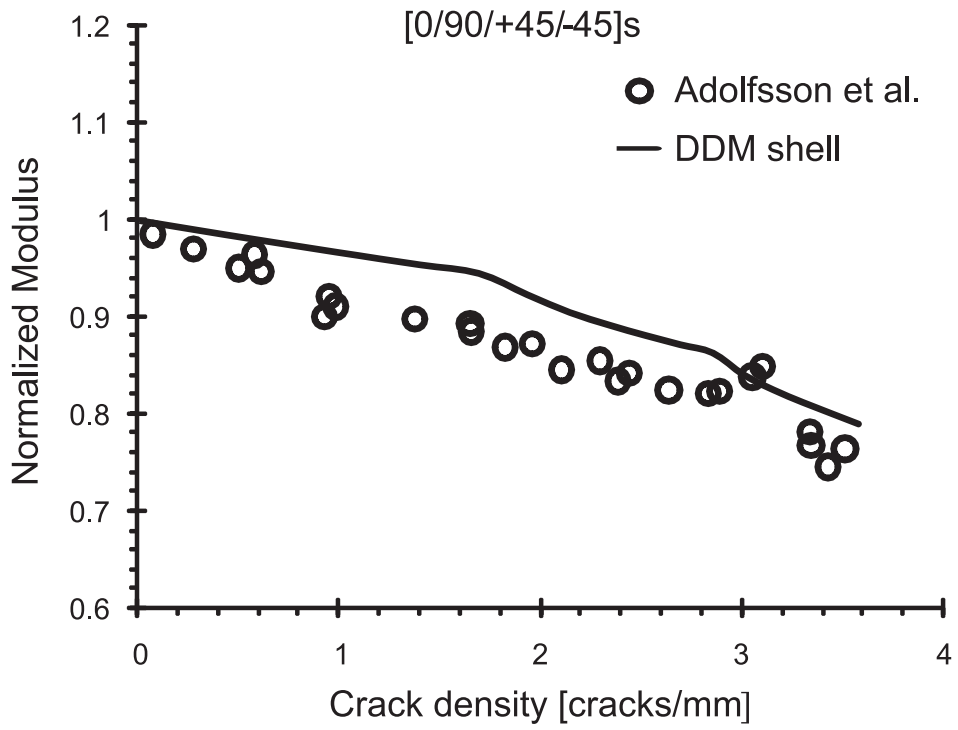

Figure 9: Normalized modulus $E_x/\bar{E}_x$ vs. crack density for a $[0_n/90_n/45_n/-45_n]_S$ laminate with $n = 1$.

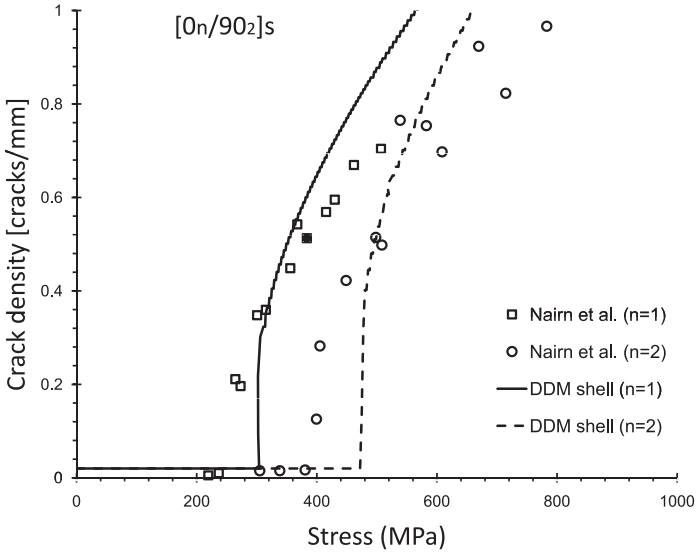

Figure 10: Crack density vs. stress for Hercules AS4/3501-6 cross-ply laminate.

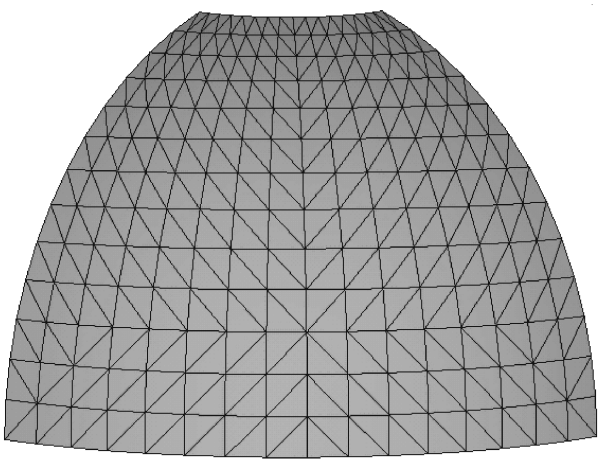

Figure 11: Cut sphere under internal pressure discretized with three-node shell elements (DDM-shell).

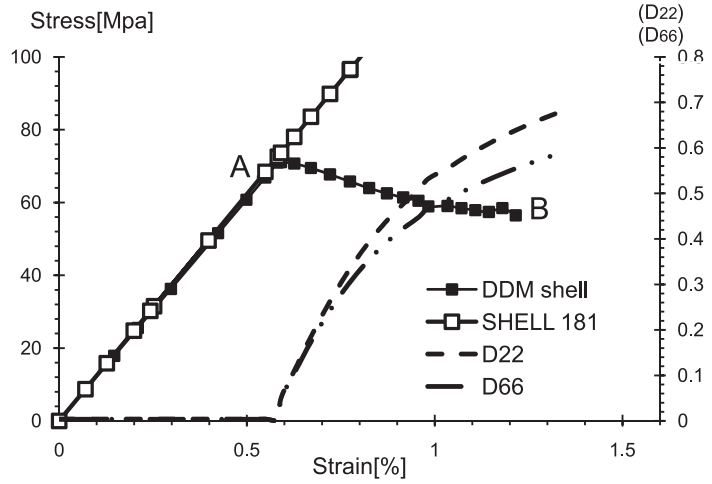

Figure 12: Strain-stress response $\sigma_{22} - \epsilon_{22}$ and damage evolution D_{22}, D_{66} in the 90° lamina.

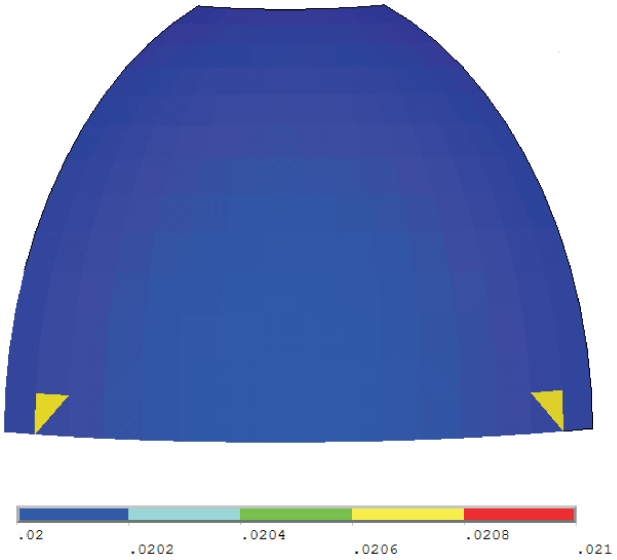

Figure 13: Crack density in the 90° lamina corresponding to point A (crack initiation) in Fig. 12.

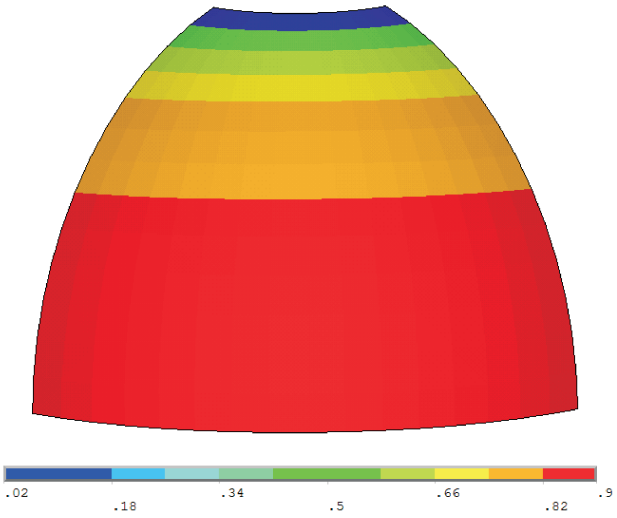

Figure 14: Crack density in the 90° lamina corresponding to point B (crack saturation) in Fig. 12.

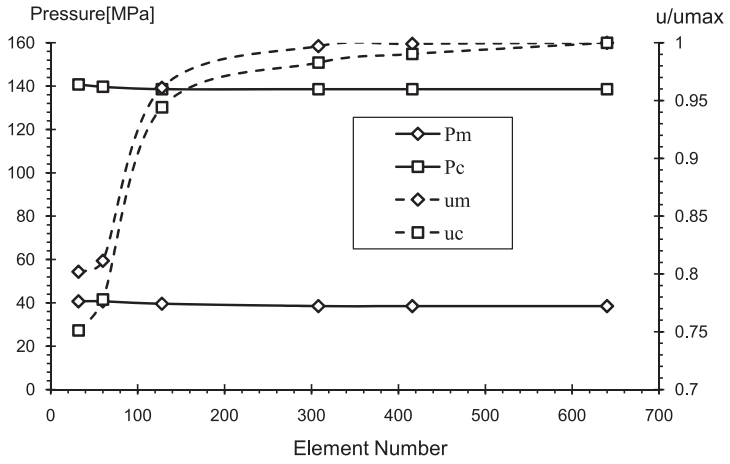

Figure 15: Convergence study.

The strain-stress response in the 90° lamina is shown in Figure 12 for the element where damage initiates. Due to symmetry, damage initiates in two elements simultaneously, as shown in Figure 13. In Figure 12, the response is compared to the linear response obtained with ANSYS SHELL 181. Also, the damage values $D_{ij}(\lambda)$ are shown in the figure. The reduction of stiffness is proportional to the damage parameters as per (20), i.e, the damage stiffness can be calculated as

$$Q_{ij}^{(k)} = \left[1 - D_{ij}^{(k)}(\lambda^{(k)})\right] \overline{Q}_{ij}^{(k)} \tag{27}$$

where $\overline{Q}_{ij}^{(k)}$ is the undamaged stiffness of lamina k.

The first element that damages is shown in Figure 13, corresponding to point A in Figure 12. Crack saturation is shown in Figure 14, corresponding to point B in Figure 12.

A plot of displacement versus the number of elements is normally used to illustrate convergence of the solution as the mesh if refined. In finite element analysis, it is expected that the displacement and stress gradients be mesh dependent until convergence is reached for a very fine mesh. A plot of the applied load required to attain a certain response (e.g., damage initiation or damage saturation) versus the number of elements is normally used to show mesh dependency that might be caused by the constitutive equation, in addition to the mesh dependency seen in the displacement.

Radial displacements of the shell and applied pressure at damage initiation (u_c, p_c) and at damage saturation (u_m, p_m) are shown in Figure 15 as a function of the number of elements used in the discretization. As it is show in the figure, the constitutive model does not suffer from mesh dependency. It can be seen that the load (pressure in this example) at which damage initiation (p_c) and damage saturation (p_m) take place, are virtually independent of the mesh refinement, even when a very coarse mesh is used. This is true even when the displacement field displays mesh dependency, as expected from a finite element discretization. The radial displacement at damage initiation (u_c) and damage saturation (u_m) reduce by about 20% from a very coarse mesh to the asymptotic value for a fine discretization. For the coarse discretization (32 elements), the mesh is barely able to model the curved geometry of the shell, thus affecting the quality of the predicted displacement field, but still not degrading at all the prediction of constitutive response. The radial displacements and stresses calculated with this element, before damage takes place, are virtually identical to those computed with ANSYS SHELL 181 (see Fig. 12).

6 Conclusions

The three-node shell element and associated constitutive model predict damage in response to membrane stress (strain) and the damage affects both the membrane and the bending stiffness of the laminate. The formulation is able to predict matrix cracking initiation, evolution and stiffness reduction for symmetric laminates with general lamina stacking sequence and it is not affected by *constitutive* mesh dependency. Excellent predictions were achieved using material properties available in the literature (including values of fracture toughness G_{Ic} and G_{IIc}). Damage is represented by the crack density in each lamina, which is a physically meaningful measure of damage. Furthermore, it is shown that the proposed formulation and its implementation are able to predict damage initiation and evolution for complex shell structures, and thus useful for practical engineering analysis.

Acknowledgements

The authors wish to thank Dr. Xavier Martinez for his insightful suggestions regarding the use of user material subroutines in commercial FEA codes. The first author acknowledges partial financial support from the Italian government for his stay at West Virginia University.

A Appendix

The transformation from the *global* (G) coordinate system to the *laminate* (L) coordinate system can be obtained using the following three matrices [2, (1.21)]

$$[\overline{a}^L_{xy}] = \begin{bmatrix} \cos\theta_{xy} & \sin\theta_{xy} & 0 \\ -\sin\theta_{xy} & \cos\theta_{xy} & 0 \\ 0 & 0 & 1 \end{bmatrix} \tag{28}$$

$$[\overline{a}^L_{yz}] = \begin{bmatrix} 1 & 0 & 0 \\ 0 & \cos\theta_{yz} & \sin\theta_{yz} \\ 0 & -\sin\theta_{yz} & \cos\theta_{yz} \end{bmatrix} \tag{29}$$

$$[\overline{a}^L_{xz}] = \begin{bmatrix} \cos\theta_{xz} & 0 & -\sin\theta_{xz} \\ 0 & 1 & 0 \\ \sin\theta_{xz} & 0 & \cos\theta_{xz} \end{bmatrix} \tag{30}$$

where the first matrix is associated to a rotation around the z′-axis, the second matrix is associated to a rotation around the rotated x′-axis, and the third matrix is associated to a rotation around the rotated y″-axis (Figure 4). The combined rotation matrix $[a]$ can be expressed as follows

$$[a] = \overline{a}^L_{xz}\overline{a}^L_{yz}\overline{a}^L_{xy} = \begin{bmatrix} a_{11} & a_{12} & a_{13} \\ a_{21} & a_{22} & a_{23} \\ a_{31} & a_{32} & a_{33} \end{bmatrix} \tag{31}$$

where

$$
\begin{array}{l}
a_{11} = \cos\theta_{xz}\ \cos\theta_{xy} - \sin\theta_{xz}\ \sin\theta_{yz}\ \sin\theta_{xy}; a_{12} = -\cos\theta_{xz}\ \sin\theta_{xy} + \sin\theta_{xz}\ \sin\theta_{yz}\ \sin\theta_{xy} \\
a_{13} = -\sin\theta_{xz}\ \cos\theta_{yz}; a_{21} = -\cos\theta_{yz}\ \sin\theta_{xy}; a_{22} = \cos\theta_{yz}\ \cos\theta_{xy}; a_{23} = \sin\theta_{yz} \\
a_{31} = \sin\theta_{xz}\ \cos\theta_{xy} + \cos\theta_{xz}\ \sin\theta_{yz}\ \sin\theta_{xy}; a_{32} = -\sin\theta_{xz}\ \sin\theta_{xy} - \cos\theta_{xz}\ \sin\theta_{yz}\ \cos\theta_{xy} \\
a_{33} = \cos\theta_{xz}\ \cos\theta_{yz}
\end{array}
\tag{32}
$$

The stress transformation matrix to transform the stress from *global* coordinate system to *laminate* coordinate system, has the form [2, (1.33)]

$$
[T^{sL}] = \begin{bmatrix}
a_{11}^2 & a_{12}^2 & a_{13}^2 & 2\ a_{12}\ a_{13} & 2\ a_{11}\ a_{13} & 2\ a_{11}\ a_{12} \\
a_{21}^2 & a_{22}^2 & a_{23}^2 & 2\ a_{22}\ a_{23} & 2\ a_{21}\ a_{23} & 2\ a_{21}\ a_{22} \\
a_{31}^2 & a_{32}^2 & a_{33}^2 & 2\ a_{32}\ a_{33} & 2\ a_{31}\ a_{33} & 2\ a_{31}\ a_{32} \\
a_{21}\ a_{31} & a_{22}\ a_{32} & a_{23}\ a_{33} & a_{22}\ a_{33} + a_{23}\ a_{32} & a_{21}\ a_{33} + a_{23}\ a_{31} & a_{21}\ a_{32} + a_{22}\ a_{31} \\
a_{11}\ a_{31} & a_{12}\ a_{32} & a_{13}\ a_{33} & a_{12}\ a_{33} + a_{13}\ a_{32} & a_{11}\ a_{33} + a_{13}\ a_{31} & a_{11}\ a_{32} + a_{21}\ a_{31} \\
a_{11}\ a_{21} & a_{12}\ a_{22} & a_{13}\ a_{23} & a_{12}\ a_{23} + a_{13}\ a_{22} & a_{11}\ a_{23} + a_{13}\ a_{21} & a_{11}\ a_{22} + a_{12}\ a_{21}
\end{bmatrix}
\tag{33}
$$

whereas the strain transformation matrix, from *global* coordinate system to *laminate* coordinate system, is obtained as [2, (1.39)]

$$
[T^{eL}] = [R][T^{sL}][R]^{-1} \tag{34}
$$

where the Reuter matrix is given in [2, (1.37)].

The transformation of the stiffness $[C]$ and compliance $[S]$ matrices from the *global* coordinate system to the *laminate* coordinate system $[C^L], [S^L]$, is performed according to the relationships [2, (1.50),(1.53)]

$$
\begin{array}{l}
[C^L] = [T^{sL}][C][T^{sL}]^T \\
[S^L] = [T^{eL}][S][T^{eL}]^T
\end{array}
\tag{35}
$$

and from *laminate to global* coordinate system as follows [2, (1.49),(1.52)]

$$
\begin{array}{l}
[C] = [T^{eL}]^T[C^L][T^{eL}] \\
[S] = [T^{sL}]^T[S^L][T^{sL}]
\end{array}
\tag{36}
$$

The transformation matrix $[a^E]$ from the *global* (G) coordinate system to the *element* (E) coordinate system contains the direction cosines of the element (local) coordinate system (r,s,t,) w.r.t the global system (X,Y,Z.) Then, the transformation matrix $[T^{sE}]$ is obtained by substituting $[a^E]$ for $[a]$ in (33). Then, to transform the strain tensor from *global to element* coordinate system we use

$$
[T^{eE}] = [R][T^{sE}][R]^{-1} \tag{37}
$$

and to transform constitutive equations from *global to element* coordinate system we use

$$[C^E] = [T^{sE}][C][T^{sE}]^T \tag{38}$$

and from the *element* to *global* coordinate system we use

$$[C] = [T^{eE}]^T[C^E][T^{eE}] \tag{39}$$

Note also that $[T^s]^{-1} = [T^e]^T$ and that $[T^e]^{-1} = [T^s]^T$.

References

[1] E. J. Barbero, Introduction to Composite Material Design–Second Edition, CRC, Boca Raton, FL, 2010.

[2] E. J. Barbero, Finite Element Analysis of Composite Materials, CRC, Boca Raton, FL, 2007.

[3] S. Pinho, C. G. Dávila, L. Iannucci, P. Robinson, Failure models and criteria for FRP under in-plane or three-dimensional stress states including shear non-linearity, NASA/TM-2005-213530 (2005).

[4] G. F. Abdelal, A. Caceres, E. J. Barbero, A micro-mechanics damage approach for fatigue of composite materials, Composite Structures 56 (4) (2002) 413–422.

[5] E. Barbero, G. Abdelal, A. Caceres, A micromechanics approach for damage modeling of polymer matrix composites, Composite Structures 67 (4) (2005) 427–436.

[6] ASTM International. Web resource.
URL www.astm.org

[7] P. Davies, Protocols for interlaminar fracture testing of composites., Polymer and Composites Task Group. European Structural Integrity Society (ESIS), Plouzané, France, 1992.

[8] R. Rikards, F. G. Buchholz, H. Wang, A. K. Bledzki, A. Korjakin, H. A. Richard, Investigation of mixed mode I/II interlaminar fracture toughness of laminated composites by using a cts type specimen, Engineering Fracture Mechanics 61 (1998) 325–342.

[9] Z. Hashin, Finite thermoelastic fracture criterion with application to laminate cracking analysis, J. Mech. Phys. Solids 44 (7) (1996) 1129–1145.

[10] J. A. Nairn, Matrix Microcracking in Composites, in Comprehensive Composite Materials, Elsevier, 2000.

[11] J. A. Nairn, Finite Fracture Mechanics of Matrix Microcracking in Composites, in The Application of Fracture Mechanics to Polymers, Adhesives and Composites, Editor: D. R. Moore, Elsevier, 2004.

[12] R. J. Nuismer, S. C. Tan, Constitutive relations of a cracked composite lamina, Journal of Composite Materials 22 (1989) 306–321.

[13] S. C. Tan, R. J. Nuismer, A theory for progressive matrix cracking in composite laminates, Journal of Composite Materials 23 (1989) 1029–1047.

[14] S. Liu, J. A. Nairn, The formation and propagation of matrix microcracks in cross-ply laminates during static loading, Journal of Reinforced Plastics and Composites 11 (1992) 158–173.

[15] J. A. Nairn, On the use of shear-lag methods for analysis of stress transfer unidirectional composites, Mecahinics of Materials 26 (2) (1997) 63–80.

[16] J. A. Mayugo, P. P. Camanho, P. Maimí, C. G. Dávila, Analytical modelling of transverse matrix cracking [+-theta/90n]s of composite laminates under multiaxial loading, Mechanics of Advanced Materials and Structures (2010) accepted.

[17] T. Yokozeki, T. Aoki, Overall thermoelastic properties of symmetric laminates containing obliquely crossed matrix cracks, Composite Science and Technology 65 (2005) 1647–1654.

[18] D. G. Katerelos, L. N. McCartney, C. Galiotis, Effect of off-axis matrix cracking on stiffness of symmetric angle-ply composite laminates, Int. J. of Fracture 139 (2006) 529–536.

[19] D. H. Cortes, E. J. Barbero, Stiffness reduction and fracture evolution of obliquely matrix cracks in composite laminates, Annal of Solid and Structural Mechanics, DOI:10.1007/s12356-009-0001-5.

[20] S. Li, S. R. Reid, P. D. Soden, A finite strip analysis of cracked laminates, Mechanics of Materials 18 (1994) 289–311.

[21] E. Adolfsson, P. Gudmundson, Thermoelastic properties in combined bending and extension of thin composite laminates with transverse matrix cracks, International Journal of Solids and Structures 34 (16) (1997) 2035–2060.

[22] E. Adolfsson, P. Gudmundson, Matrix crack initiation and progression in composite laminates subjected to bending and extension, International Journal of Solids and Structures 36 (1999) 3131–3169.

[23] L. N. McCartney, Energy-based prediction of progressive ply cracking and strength of general symmetric laminates using an homogenization method, Composites Part A 36 (2005) 119–128.

[24] L. N. McCartney, Energy-based prediction of failure in general symmetric laminates, Engineering Fracture Mechanics 72 (2005) 909–930.

[25] R. Zinno, F. Greco, Damage evolution in bimodular laminated composites under cyclic loading, Composite Structures 53 (2001) 381–402.

[26] A. Tessler, An improved plate theory of 1,2-order for thick composite laminates, Int. J. Solids and Structures 30(7) (1993) 981–1000.

[27] ANSYS User's Manual, release 12, Canonsburg, PA.

[28] A. Tessler, E. Saether, T. Tsui, Vibration of thick laminated composite plates, J. Sound and Vibration 179(3) (1995) 475–498.

[29] J. W. Mohr, Efficient triangular shell elements for thick composite and sandwich laminates, M.S. thesis, George Washington University, 2000.

[30] K. J. Bathe, Finite Element Procedures, second ed., Prentice-Hall, 1995, first ed. ISBN 9780979004902 (1982).

[31] E. J. Barbero, D. H. Cortes, A mechanistic model for transverse damage initiation, evolution, and stiffness reduction in laminated composites,, Composites Part B.
URL http://dx.doi.org/10.1016/j.compositesb.2009.10.001

[32] E. J. Barbero; G. Sgambitterra; A. Adumitroaie; X. Martinez, A Discrete Constitutive Model for Transverse and Shear Damage of Symmetric Laminates with arbitrary Stacking Sequence, Composite Structures, 2010, DOI: 10.1016/j.compstruct.2010.06.011.

[33] T. Yokozeki, T. Aoki, T. Ishikawa, Consecutive matrix cracking in contiguous plies of composite laminates, International Journal of Solids and Structures 42 (2005) 2785–2802.

[34] T. Yokozeki, T. Aoki, T. Ogasawara, T. Ishikawa, Effects of layup angle and ply thickness on matrix crack interaction in contiguous plies of composite laminates, Composites Part A: Applied Science and Manufacturing 36 (2005) 1229–1235.

[35] R. Talreja, Damage Characterization by Internal Variables, in Damage Mechanics of Composite Materials, Elsevier Science, 1994.

[36] S. Li, S. R. Reid, P. D. Soden, A continuum damage model for transverse matrix cracking in laminate fiber-reinforced composites, Philosophical Transaction of the Royal Society of London. A 356 (1998) 2379–2412.

[37] E. J. Barbero, L. DeVivo, A constitutive model for elastic damage in fiber-reinforced pmc laminae, J. of Damage Mechanics 10 (2001) 73–93.

[38] S. Oller, E. O. ate, J. Miquel-Canet, S. Botello, A plastic damage constitutive model for composite materials, International Journal of Solids and Structures 33(17) (1996) 2501–2518.

[39] H. T. Hahn, A mixed-mode fracture criterion for composite materials, Journal of Composites Technology and Research 5 (1983) 26–29.

[40] J. Varna, R. Joffe, N. V. Akshantala, R. Talreja, Damage in composite laminates with off-axis plies, Composite Science and Technology 59 (1999) 2139–2147.